

Chapter 1

Experimental

In this work two complementary surface science techniques, LEED and STM, were used. With Low-Energy Electron Diffraction (LEED) one probes the k space and extracts information on the symmetry, the surface unit cell dimensions and the atomic roughness of a surface. The diffraction pattern contains information averaged over a macroscopic surface area of about 12 mm^2 (size of the electron spot on the surface). Scanning Tunneling Microscopy (STM), on the other hand, is capable of mapping the local surface structure in real space with atomic resolution. These two methods are a very good combination and complement one another.

In the following chapter I will discuss the essential theoretical basics of both methods necessary to understand and discuss the obtained data. More detailed information can be found in the cited literature sources (e.g. [Bai88] for STM, [HWC85] and [Hor99] for LEED). Furthermore, I will describe the STM and Spot Profile Analysis-LEED (SPA-LEED) instruments as well as the sample preparation procedures.

1.1 Scanning Tunneling Microscopy

There are many publications ([Bai88] and references in there) about the theory of the Scanning Tunneling Microscope invented by Gerd Binnig and Heinrich Rohrer in 1981 [BRGW82a, BRGW82b]. I will follow the theory of Tersoff and Hamann [TH85], which is based on Bardeen's formalism [Bar61]. This first-order perturbation theory approach leads to a tunneling current between two electrodes separated by a vacuum gap, which is given by

$$I = \frac{2\pi e}{\hbar} \sum_{\mu,\nu} f(E_\mu) [1 - f(E_\nu + eV)] |M_{\mu\nu}|^2 \delta(E_\mu - E_\nu), \quad (1.1)$$

where $f(E)$ is the Fermi function, V is the applied voltage, $M_{\mu\nu}$ the tunneling matrix element between states ψ_μ of the probe and ψ_ν of the surface, and $E_{\mu,\nu}$ is the energy of the state $\psi_{\mu,\nu}$ in the absence of tunneling.

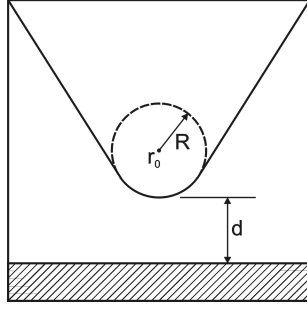


Figure 1.1: Schematic picture of the tunneling geometry [TH85]

For this general expression several approximations are necessary to achieve a practical format. The results of some essential approximations are shown in the following.

Usually experiments are performed at room temperature or below and with small tunneling voltages (~ 10 meV for metal-metal tunneling). Here, the Fermi function $f(E)$ is considered as a Heaviside function, which is especially reasonable for low temperature tunneling. Considering these conditions, equation 1.1 leads to

$$I = \frac{2\pi}{\hbar} e^2 V \sum_{\mu, \nu} |M_{\mu\nu}|^2 \delta(E_\nu - E_F) \delta(E_\mu - E_F), \quad (1.2)$$

with E_F as the Fermi energy.

One problem for all formalisms used to describe the tunneling process is the tip. Usually there is no reliable information accessible about the microscopic geometry of the tip. Often it is prepared in an uncontrolled and non-reproducible manner by establishing mechanical contact between the tip and the metallic sample. (For non-metallic surfaces other tip modifications have to be used, but the tip shape is also not well known in this case.) Therefore a feasible model for the tip has to be applied to the problem. Considering a limiting case, where the tip is treated as a point probe, equation 1.2 reduces to

$$I \propto \sum_{\nu} |\psi_{\nu}(\vec{r}_0)|^2 \delta(E_\nu - E_F). \quad (1.3)$$

The expression on the right is the surface local density of states (LDOS) at E_F . When the STM operates in the constant current mode, which is the most common imaging procedure, the obtained image represents a contour map of constant surface LDOS.

The assumption for the tip as a point probe needs to be replaced by a more realistic model, where the tip is locally spherical with a radius of curvature R and the distance of nearest approach is d (see Figure 1.1).

The matrix element from equation 1.2 is evaluated for an s-wave tip wave function. This

approach leads to the result

$$I = 32\pi^3 \hbar^{-1} e^2 V \phi^2 D_t(E_F) R^2 \kappa^{-4} e^{2\kappa R} \sum_{\nu} |\psi_{\nu}(\vec{r}_0)|^2 \delta(E_{\nu} - E_F), \quad (1.4)$$

where D_t is the density of states per unit volume of the probe tip, and $\kappa = \hbar^{-1}(2m\phi)^{1/2}$ is the minimum inverse decay length for the wave function in vacuum with ϕ as the work function of the surface. With typical values for metals, one obtains for the tunneling conductance

$$\begin{aligned} \sigma &= 0.1 R^2 e^{2\kappa R} \rho(\vec{r}_0, E_F) \quad \text{with} \\ \rho(\vec{r}_0, E) &\equiv \sum |\psi_{\nu}(\vec{r}_0)|^2 \delta(E_{\nu} - E), \end{aligned} \quad (1.5)$$

where σ is in Ω^{-1} , distances in a.u., and the energy E in eV. If we substitute

$$|\psi_{\nu}(\vec{r}_0)|^2 \propto e^{-2\kappa(R+d)} \quad (1.6)$$

into equation 1.5, we obtain the expected result:

$$\sigma \propto e^{-2\kappa d} \quad (1.7)$$

For an applied voltage the tunneling current is exponentially dependent on the distance between tip and sample.

1.2 Low-Energy Electron Diffraction

For over 80 years electron diffraction has proven to be a powerful method for surface analysis [Cla85]. The de Broglie wavelength of electrons is given by

$$\lambda = \sqrt{\frac{h^2}{2m_e E}} \quad \Longrightarrow \quad \lambda[\text{\AA}] = \sqrt{\frac{150.4}{E[\text{eV}]}}. \quad (1.8)$$

For energies between 10 eV and 500 eV, the electron wavelength is in the range of the inter-atomic distance in typical crystal structures. Furthermore, in this energy range the penetration depth of electrons is limited to only a few atomic layers [EK85]. Therefore, Low-Energy Electron Diffraction (LEED) is a surface-sensitive method and the most widely used technique for the analysis of surface crystal structures.

A LEED pattern obtained from a long-range ordered surface contains different kinds of information: The position and total intensity of the diffracted electron beam, and the intensity profile $I(k_{\parallel})$ of the beam measured at a fixed energy. There are two major approaches to extract information from a LEED pattern: The *kinetic theory*, where only single scattering events are considered, and the *dynamic theory* with multiple scattering events. Electrons in the LEED range

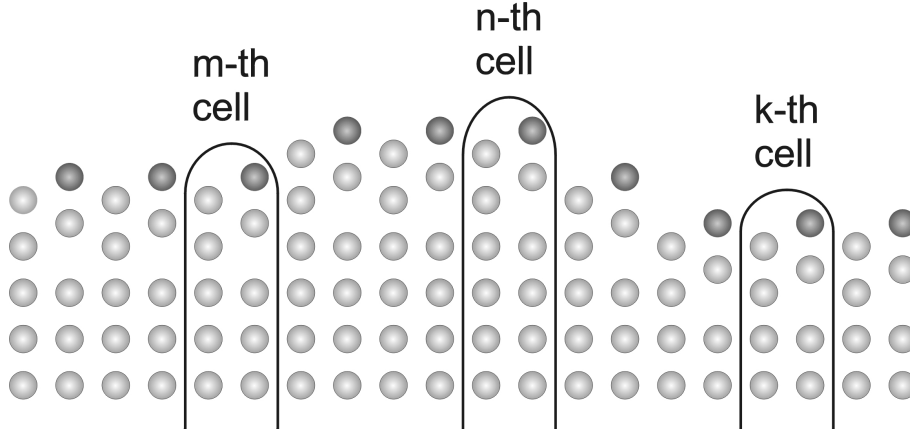


Figure 1.2: Arrangement of identical surface unit cells [Hen84]

of 10 eV to 500 eV have a penetration of 5 Å to 20 Å [HG91]. LEED is therefore surface sensitive, but it causes multiple scattering events, which need to be considered for a full computation of the total intensity of LEED spots. It is the domain of the dynamic theory to calculate these total intensities and to derive information on the atomic structure within a surface unit cell. In the kinetic theory, on the other hand, the spot profile is evaluated and information on the arrangement of identical surface unit cells is derived (atomic surface roughness). This approach is briefly discussed in the following [Hen84].

The diffraction from a surface can be described as the sum of electron waves scattered from the initial wave vector \vec{k}_i of the incoming electron to the final wave vector \vec{k}_f by all surface atoms at the positions \vec{r}_n :

$$\Psi(\vec{K}, \vec{k}_i) = \sum_n f(\vec{r}_n, \vec{K}, \vec{k}_i) e^{i\vec{K}\vec{r}_n}, \quad (1.9)$$

with $\vec{K} = \vec{k}_i - \vec{k}_f$ as the scattering vector and $f(\vec{r}_n, \vec{K}, \vec{k}_i)$ as the structure factor. The intensity of the diffraction spots is subsequently:

$$I(\vec{K}, \vec{k}_i) = |\Psi(\vec{K}, \vec{k}_i)|^2. \quad (1.10)$$

For the kinematic approximation the individual structure factors $f(\vec{r}_n, \vec{K}, \vec{k}_i)$ will be replaced by one structure factor $f(\vec{K}, \vec{k}_i)$ under the assumption that the surface consists of identical unit cells. These identical cells can be seen as the columns indicated in Figure 1.2. Within this approximation, which is strictly valid only for a smooth and flat surface, the intensity I splits up into:

$$I(\vec{K}, \vec{k}_i) = |\Psi(\vec{K}, \vec{k}_i)|^2 = F \cdot G \quad \text{with} \quad (1.11)$$

$$F = |f(\vec{K}, \vec{k}_i)|^2 \quad \text{as the dynamic form factor, and} \quad (1.12)$$

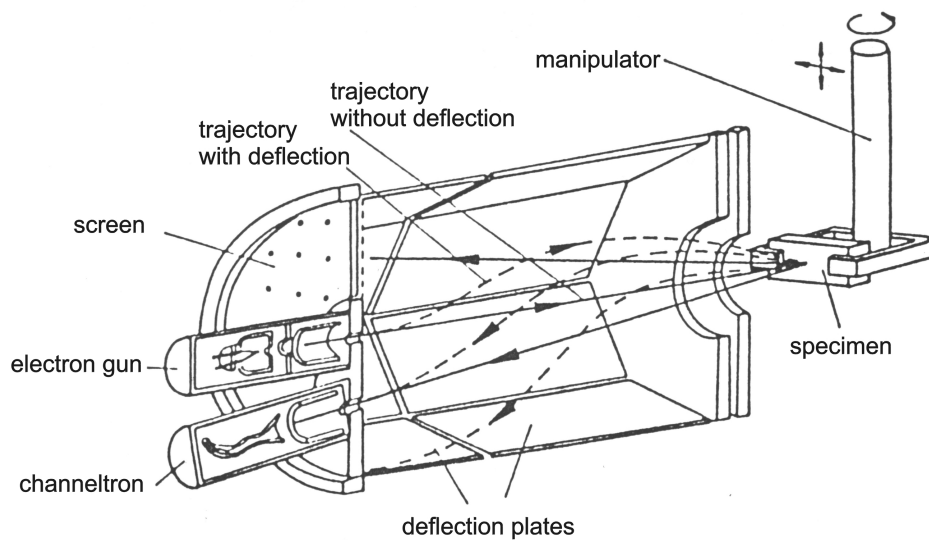


Figure 1.3: Schematic set-up of the SPA-LEED system

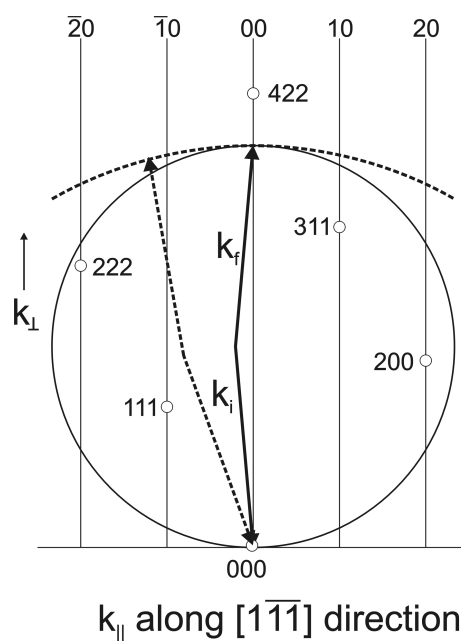


Figure 1.4: Scattering geometry for the SPA-LEED instrument

the angle between the wave vectors \vec{k}_i and \vec{k}_f remains constant at 4° ; the situation is equivalent to a sample rotation with fixed positions of the detector and the source

$$G = \left| \sum_n e^{i\vec{K}\vec{r}_n} \right|^2 \quad \text{as the lattice vector.} \quad (1.13)$$

The lattice factor G corresponds to the Fourier transform of the surface lattice and contains all information on the arrangement of identical surface unit cells. It can be determined from the experimentally measured intensity $I(k_{\parallel}, k_{\perp})$ by a normalization to the total intensity I_{total} ¹:

$$\frac{I(k_{\parallel}, k_{\perp})}{I_{total}} = \frac{F(\vec{K}, \vec{k}_i) \cdot G(k_{\parallel}, k_{\perp})}{\int_{BZ} F(\vec{K}, \vec{k}_i) \cdot G(k_{\parallel}, k_{\perp}) dk_{\parallel}} \quad (1.14)$$

$$\sim \frac{F(\vec{K}, \vec{k}_i) \cdot G(k_{\parallel}, k_{\perp})}{\overline{F}_{BZ} \int_{BZ} G(k_{\parallel}, k_{\perp}) dk_{\parallel}} \quad (1.15)$$

$$= \frac{F(\vec{K}, \vec{k}_i) \cdot G(k_{\parallel}, k_{\perp})}{\overline{F}_{BZ}} \quad (1.16)$$

$$\sim G(k_{\parallel}, k_{\perp}) \quad (1.17)$$

with the assumption that the dynamic form factor F does not vary significantly within the surface Brillouin zone (BZ).

In 1986 Henzler et al. [SMH86] developed a new instrument for the Spot Profile Analysis of Low-Energy Electron Diffraction (SPA-LEED), which can be seen schematically in Figure 1.3. With this instrument the transfer width was increased up to 200 nm, i.e. periodic structures with a separation up to this length can be resolved. Due to channeltron detection, the intensity can be measured over a range of six orders of magnitude. The scattering geometry for this instrument can be seen in Figure 1.4. During a scan at a fixed energy, the angle between the incident electron wave vector \vec{k}_i and the (00) lattice rod is changed by means of the deflection unit between electron gun and sample (cf. Figure 1.3). The angle between the wave vectors \vec{k}_i and \vec{k}_f remains constant at 4°. Hence, the scattering geometry is equivalent to a situation where the sample is rotated and the position of source and detector remains fixed. An important information which can be directly extracted from the spot profile is average terrace length of a atomically rough surface. In this case, the important quantity is the full width at half maximum measured at an out-of-phase scattering condition [Hen78, WFH90]. Under the assumption that coherent scattering between different terraces is negligible, the half width Δk_{\parallel} directly yields the average terrace width $\Gamma = \frac{2\pi}{\Delta k_{\parallel}}$.

The shape and inclination of the reciprocal lattice rods contains direct information on the topography of a surface with a modulated roughness (i.e. a faceted surface) [Hen84, Hor99]. Figure 1.5a shows an exemplary surface configuration of a simple-cubic crystal with flat and faceted areas. The normal orientation of this surface is (100), whereas the facets have a (110)

¹The total intensity of the diffuse broadening and the central spike of a particular spot (i j) is conserved, independent of k_{\perp} (electron energy), and normalized to 1: $\int_{BZ} G_{ij}(\vec{K}) d\vec{k}_{\parallel} = 1$.

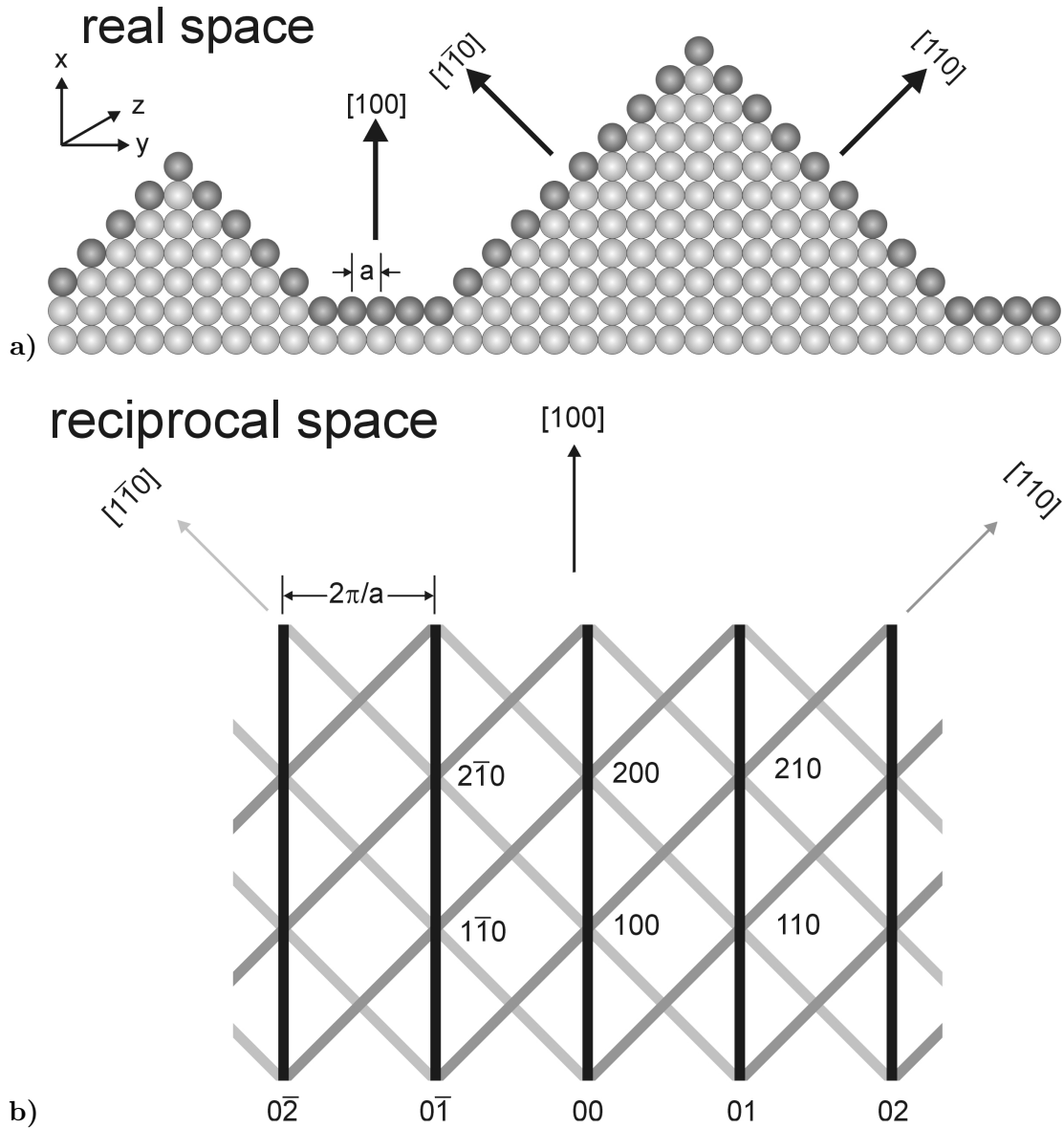


Figure 1.5: Facet arrangement at the (100) surface of a simple-cubic crystal with the respective lattice rods

a) faceted surface with flat (100) oriented areas, and with (110) and ($1\bar{1}0$) facets

b) respective lattice rods of the facet structure in a) with vertical lattice rods of (100)-oriented areas and inclined facet rods of the (110) and the ($1\bar{1}0$) facets

and a $(1\bar{1}0)$ orientation. The corresponding lattice rods in reciprocal space can be seen in Figure 1.5b. The flat areas of the surface are represented by vertical lattice rods along the $[100]$ surface normal, whereas the facets are represented by inclined facet rods along the $[1\bar{1}0]$ and the $[110]$ direction. The points in reciprocal space where all three sets of lattice rods intersect correspond to the Bragg points of the crystal lattice. From the Bragg indices of the intersection points, the facet orientations can be easily determined. With the help of SPA-LEED, the intensity distribution $I(k_{\parallel}, k_{\perp})$ along the lattice rods is directly accessible by mapping the scattered intensity along respective planes in reciprocal space. Hence, SPA-LEED is particularly well suited for the quantitative evaluation of faceted surfaces.

1.3 UHV Systems and Sample Preparation

The experiments for my work were performed using electron diffraction and scanning tunneling microscopy. For the investigations, two separate ultra-high vacuum (UHV) chambers were available, one of which contained a High-Resolution Low-Energy Electron Diffraction (SPA-LEED) system as the main component while the other UHV system contained a homebuilt low-temperature Scanning Tunneling Microscope (STM). All experiments were performed at a base pressure lower than $3 \cdot 10^{-10}$ mbar.

1.3.1 SPA-LEED System

The SPA-LEED instrument was a commercial Omicron optics. Disc-shaped samples with a diameter of 6 mm were mounted on a resistive heater, which was fixed to the manipulator. The manipulator allowed lateral and vertical movement as well as azimuthal and polar rotation to adjust the sample position in the desired orientation. The manipulator was designed to enable cooling of the sample down to about 100 K using liquid N_2 . For sample cleaning, a sputter gun with a direct Ne gas inlet was available. A quadrupole mass spectrometer was used to analyze the residual gas pressure in the UHV chamber. Annealing of the sample was performed using the resistive heater and could be monitored with a NiCr/Ni thermocouple attached to the heater/sample connection.

For the deposition of materials, two different types of evaporators were available in the SPA-LEED chamber, namely Al_2O_3 crucibles for the thermal sublimation of the alkali halide deposits and a water-cooled electron beam evaporator for metal deposition. An X-ray source ($Al-k_{\alpha}$, $Mg-k_{\alpha}$) in combination with a hemispherical electron energy analyzer allowed to perform X-ray photoelectron spectroscopy (XPS). In this way, the chemical composition and the coverage of the alkali halide films were monitored.

1.3.2 LT-STM System

The low-temperature STM used for this study is based on the design by G. Meyer [Mey96, Zöp00] with supplementary modifications by K.-F. Braun [Bra01]. The UHV system consisted of two chambers, a preparation chamber and an STM chamber. Equivalent to the SPA-LEED system, the sample was mounted on a resistive heater attached to a sample holder. This sample holder could be transferred between the two chambers with the manipulator, which could be cooled with liquid Helium or N₂. The preparation chamber was equipped with a sputter gun, a mass spectrometer, a conventional LEED optics, and metal and alkali halide evaporators. Gas adsorbates could be dosed by a leak valve. The STM chamber consisted of a bath cryostat with two tanks of liquid N₂ and liquid He, which cools the sample down to the measurement temperature of 6 K. The scanner of the STM works according to the Besocke type [Zöp00]. Cut PtIr STM tips were used throughout this study. All bias voltages mentioned in the following correspond to the sample voltage with respect to the tip.

1.3.3 Sample Preparation

The samples were chemomechanically polished crystals purchased from Fa. Mateck. The preparation of the samples under UHV conditions consisted of repeated Ne⁺ sputtering cycles at energies between 900 eV and 1300 eV and currents of typically 5 μ A. Subsequently to the sputtering, the samples were annealed at temperatures between 650 K and 900 K. The preparation of the kinked Cu(532) surface was carried out by applying different temperature ramps during the cooling procedures after the annealing process to promote an ordering of the kink atoms. The specific values for the annealing temperatures are listed in Table 1.1.

Sample orientation	Temperature
Cu(311)	650 K
Cu(221)	750 K
Ag(211)	900 K
Cu(532)	850 K

Table 1.1: Annealing temperatures for the sample preparation

The alkali halides (99.95% purity) were evaporated from Al₂O₃ crucibles at about 1000 K source temperature. Under these conditions, alkali halides sublime in molecular form [REK59], which was confirmed by XPS. The coverage determination of the alkali halide deposit was performed by calibration of the XPS intensities with previous reference measurements. The error for the film thickness is assumed to be around 10%.

1.3.4 Calibration

Calibrations were also performed for the length scale in real space (STM) and in reciprocal space (SPA-LEED) with reference samples. The STM length scale was adjusted according to the nearest-neighbor distance of 2.89 \AA in atomically resolved images of an Ag(111) surface. Nevertheless, an error of 10% for the length scale in the STM images has to be taken into account due to hysteresis effects of the piezo tubes in the STM scanner and other thermal effects. For SPA-LEED, the reciprocal nearest-neighbor distance (2.46 \AA^{-1}) and the reciprocal intrinsic step distance (1.00 \AA^{-1}) of the Cu(211) sample were used for the calibration. The accuracy for the determination of reciprocal lengths from the diffraction patterns is estimated as 1.5%.

1.3.5 Image Editing

The diffraction patterns recorded with the SPA-LEED system were distorted at the outer parts due to non-ideal characteristics of the deflection unit for higher k_{\parallel} values. A correction of the diffraction patterns was possible with a program developed by W. Theis [The02]. In this program the spot positions of the surface unit cell for a known surface configuration are calculated. With these values the distortion of the diffraction pattern was compensated. Afterwards, the quantitative analysis of the diffraction patterns was performed.

The STM program by G. Meyer allows several image editing procedures. Some of the recorded STM images were smoothed by applying the low-pass filter to eliminate high-frequency noise. Another filter used was the Laplace-filter. This filter produces an image which is the second derivative of the original image. The effect of the Laplace filter is that long-wavelength modulations are suppressed, which e.g. emphasizes the illustration of the edges for the pyramidal facet structure (cf. chapter 6). The program has a built-in procedure to display the STM image in a 3-dimensional view, which was used for some representations of STM images.